

Sodium reordering transition in sodium cobaltate

D.J.P. Morris,^{1,*} M. Roger,² M.J. Gutmann,³ J.P. Goff,⁴ D.A. Tennant,^{1,5} D. Prabhakaran,⁶

A.T. Boothroyd,⁶ E. Dudzik,¹ R. Feyerherm,¹ J.-U. Hoffmann,¹ and K. Kiefer¹

¹*Hahn-Meitner-Institut Berlin, Glienicker Str. 100, D-14109 Berlin, Germany.*

²*Service de Physique de l'Etat Condensé,*

(CNRS/MIPPU/URA 2464), DSM/DRECAM/SPEC,

CEA Saclay, P.C. 135, F-91191 Gif Sur Yvette, France.

³*ISIS Facility, Rutherford Appleton Laboratory,*

Chilton, Didcot, Oxon OX11 0QX, UK.

⁴*Department of Physics, Royal Holloway,*

University of London, Egham, Surrey TW20 0EX, UK.

⁵*Institut für Festkörperphysik, Technische Universität Berlin,*

Hardenbergstrasse 36, Berlin D-10623, Germany.

⁶*Clarendon Laboratory, Parks Road, Oxford OX1 3PU, UK.*

(Dated: July 19, 2022)

Abstract

The sodium ordering in Na_xCoO_2 in the vicinity of room temperature is rationalised at high x in terms of phase transitions between square and striped phases. A complicated hexagon-of-hexagon diffraction pattern observed for $x=0.78$ can be reproduced using coexisting square and striped phases that are related by simple shear deformations. All compositions exhibit a partial melting transition to a disordered stripe phase just below room temperature, which dramatically alters the topology of the electrical conduction pathways.

Sodium Cobaltate, Na_xCoO_2 , has attracted much interest due to its wide variety of properties such as strong thermopower [1, 2], superconductivity when hydrated [3], and unexpected 3D magnetism [4, 5]. These properties can be controlled by intercalation of sodium via electrochemical techniques [6], and are strongly x dependant. Subsequently sodium ordering has been observed using electron, hard x-ray, and neutron diffraction [7, 8, 9, 10]. The underlying ordering principles can be understood by considering electrostatic interactions of sodium ions with each other and with the cobalt and oxygen ions [9].

The structure of this system creates two different environments for the sodium: Na1 which lies between adjacent cobalt ions, and Na2 which sits on a lower energy site at the center of a cobalt trigonal prism. The delicate balance between these interpenetrating hexagonal lattices causes the vacancies on the sodium layer to become attractive at short distances. Long range Coulomb interactions then allow these vacancy clusters to order over long range leading to observable superstructure peaks. This Na^+ ordering buckles the CoO_2 layer away from the occupied nearest-neighbour sodium sites (Na1) allowing cages to form within which the sodium ions are able to rattle. Meanwhile the Coulomb landscape on the cobalt layer is modified allowing narrow conduction pathways, and leading to strong correlation of the electrons. Both of these properties mean this is a phonon-glass-electron-crystal in agreement with studies of $\text{Na}_{1.2-x}\text{Ca}_x\text{Co}_2\text{O}_4$ and $\text{Li}_{0.48}\text{Na}_{0.35}\text{CoO}_2$ [11, 12] but with a ‘rattler’ site and help explain the high thermopower in this system. Variations in the Coulomb landscape are expected to lead to the mixed valancy states as observed by NMR [13, 14] and possible trapping of spins in the minima. Further observation and understanding of superstructures at different concentrations, and of the relevant transitions, will lead to greater insight into the overall control exerted on the system by the ionic ordering.

Whereas Ref. [9] was mainly focused on low temperature ordering, in the range $0.75 < x < 0.92$, we concentrate here on the evolution of the sodium order as the temperature is increased. Unexpectedly we do not observe, in the same composition range, a simple fusion with disappearance of long-range order at some critical temperature but a rearrangement of the sodiums from “square” long range order to striped order at $T=285\text{K}$ (as reported in [9], the low temperature cell is a slightly deformed square with internal angles close to but not equal to 90° that we denote by “square cell” for simplicity). Striped order continues to exist, well above room temperature, at least up to $T=350\text{K}$. The reordering of the sodiums is accompanied by a change of the potential exerted by the sodium superstructure on the

Cobalt sites. This has a drastic influence on the topology of the conducting paths (–which have now a unidimensional profile–) for the mobile carriers in the Co planes.

Single crystals of sodium cobaltate were grown using the floating zone technique in Oxford [15, 16] and then cleaved to produce high quality samples. Neutron diffraction measurements were carried out on the SXD diffractometer at ISIS and also on the flat-cone diffractometer E2 at HMI. Complementary hard X-ray diffraction on MAGS at BESSY was carried out with X-ray energy of 12.398keV giving penetration of the sample allowing the bulk ordering to be probed. SXD uses the neutron time-of-flight Laue method along with 2π steradians coverage of solid angle by position sensitive detectors to sample large volumes of reciprocal space [17]. This provides an overview of the superstructure peaks across many Brillouin zones which were then resolved at higher \mathbf{Q} -resolution using E2. Sample conditions on SXD were controlled using a closed-cycle He refrigerator and by a variable temperature cryostat on E2. Three single crystals of nominal composition $x = 0.75$, $x = 0.92$, $x = 0.78$, were investigated at different temperatures. The superstructure for $x = 0.75$ and 0.92 at 150K are reported in Ref. [9].

All three samples show very similar spectra at T=350K. However, at low temperature (T=150K), the $x = 0.78$ single crystal showed a striking “hexagon-of-hexagon” superstructure, different from that obtained in both $x=0.75$ and $x=0.92$ samples [9]. Figure 1(e) shows the hexagon-of-hexagon superstructure pattern that surrounds the hexagonal Bragg peak positions on the L=7 plane for the $x=0.78$ SXD data. The data shows a delicate l -dependence (fig. 1(a-d)) with the superstructure appearing around the Bragg positions that agree with $h + 2k \neq 3n$ & l =even over the range of l measured and then around all Bragg positions for odd l values below $l=11$ (superstructure peak intensities are sometimes weak around the $h + 2k \neq 3n$ positions) and for $h + 2k = 3n$ & $l=11$. All planes show inplane modulations of peak intensity towards or away from the $(00l)$ position indicative of buckling of the CoO_2 plane [9].

The first step in understanding the results is to realise that the $x=0.78$ data set can be indexed on a $(\frac{1}{15}\mathbf{a}^* \times \frac{1}{15}\mathbf{b}^*)$ grid. A fraction of the peaks can be identified as coming from the square lattice in Fig. 2(a) and these points were removed from Reverse Monte Carlo (RMC) calculations. RMC simulations have been performed using the integrated intensities of neutron diffraction peaks on this grid. Starting with a random distribution of Na on

the Na2 site within the real space supercell the initial value of $E = \sum_i [F_i^{exp} - F_i^{calc}]^2$ is evaluated, where $F_i^{exp/calc}$ are the normalised experimental and calculated peak intensities. At random a Na⁺ ion is moved onto an allowed vacancy and the configuration accepted if $E_{new} < E_{old}$ otherwise it is accepted with probability $P = \exp -\beta(E_{new} - E_{old})$. These integrated intensities are obtained using the 3D-integration algorithm in the SXD2001 software [18]. The absence of significant intensity for most superstructure reflections away from the hexagonal reciprocal lattice points, leads naturally to a multi-vacancy cluster pattern. For $x=0.78$, this approach gave stripes of trivacancies condensing into long-range order with cell vectors $\mathbf{a}' = 5\mathbf{b} - \mathbf{a}$ and $\mathbf{b}' = 5\mathbf{b} - 4\mathbf{a}$ (see fig. 2(c)). Phase separation is a known phenomena in this material [19].

This stripe structure is a simple modification of the square lattice requiring only two shear distortions, of one lattice spacing each, to the supercell to reach this end structure (see intermediate figure 2b). The buckling of the CoO₂ plane induced by the sodium superstructure has a maximum distortion along the c axis of $0.025c$. Fourier transforms of this are then added to the Fourier transforms of the square cell in a ratio of $\frac{I_{Stripe}}{I_{Square}}=1.3$. This summation produces remarkable agreement with this complex data set (see comparison in fig 1). Full details of the RMC simulations will be reported elsewhere.

The ground state energies, within the electrostatic model of Ref. [9], were calculated for both striped phases represented in Figs. 2(b) and 2(c). They differ by less than 1meV, which is not significant.

The patterns at 350K look quite different from those of Ref. [9], at T=150 K, with changes of symmetry suggesting a phase transition. The superstructure pattern above this transition could be labeled on a $(\frac{1}{5}\mathbf{a}^* \times \frac{1}{5}\mathbf{b}^*)$ grid. Figure 3 shows the L=7, L=10, L=11 cuts obtained for the $x=0.75$ samples at T=350K. Again the pattern shows a similar delicate l and inplane dependence.

X-ray data shows a pronounced hysteresis of over 10K between heating and cooling runs (fig. 4). Here $\mathbf{Q}=(0.65, 0.73, 0)$ and $(0, 1.33, 0)$ are from the square phase in Fig. 2(a), whereas the peak at $\mathbf{Q}=(0.8, 0, 0)$ is where the scattering is expected for either of the striped phases in Figs. 2(c) and (d). There is a highly unusual peak in the cooling run for $\mathbf{Q}=(0.8, 0, 0)$ indicating that the scattering from the high-temperature phases increases before disappearing below T=274K.

The trivacancy clusters can sit on three possible sites within the stripes in Fig. 2(c). Consider a model where the ordering of stripes is long range, but the ordering of trivacancy clusters within the stripes is not coherent from one stripe to the next. The supercell vectors for this phase are $\mathbf{a}' = 5\mathbf{b} + (\eta - 1)\mathbf{a}$ and $\mathbf{b}' = 5\mathbf{b} + (\eta - 4)\mathbf{a}$ where $\eta = 0, \pm 1$ at random. A section of this partially disordered structure is shown in Fig. 2(d). Simulations of the scattering intensity from this phase are in excellent agreement with the experimental data for $x=0.75, 0.78$ and 0.92 at elevated temperature, see for example Fig. 3. Therefore, the phase transformation is a melting transition from the long-range ordered square or striped phases in Figs. 2(a) and (c) respectively, to the disordered stripe phase in Fig. 2(d). The anomalous peak in the cooling run at $\mathbf{Q} = (0.8, 0, 0)$ can also be explained within this framework as the disordered stripe orders below 278K giving greater intensity to this superstructure peak and then reorientates into the observed square lattice below 274K. If the disordered stripes in Fig. 2(d) transform to the intermediate ordered stripe phase in Fig. 2(c), stronger scattering is expected at the same position in reciprocal space, as observed in Fig. 4(a).

We note that a different model with quadrivacancy clusters was previously proposed for the high-temperature phase [9]. However, the model proposed here is a more satisfactory explanation due to the simplicity of the phase transformations in fig. 2 and also agrees with quantitative RMC analysis. All phases have the same multi-vacancy cluster type (trivacancy) and the concentration x in each phase is the same.

Finally, the phase transition on heating to the disordered stripe phase Fig 2(c) to 2(d) is somewhat simplistic and could also include static (due to defects) or dynamic disorder. The number of stripes is approximately $\sqrt{N_{clust}}$, where N_{clust} is the number of vacancy clusters, and the average stripe length $l_{stripe} \propto \sqrt{N_{clust}}$ giving an entropy change per cluster of $\Delta S \approx k_B \sqrt{N_{clust}} \ln 3$ where each stripe has three possible longitudinal phases. The energy of mismatch between neighboring stripes will be the phase mismatch energy per cluster E_ϕ times the stripe length giving total energy change $\Delta E \approx E_\phi N$. This will always dominate the entropy change in the free energy $F = E - TS$ in the thermodynamic limit and so the disordering is driven by additional lateral degrees of disordering of the stripes and longitudinal disordering of the clusters within stripes coming into play. In this respect the phase transition resembles that of a crystal stripe phase to a smectic phase. The relatively small changes in entropy involved in the transitions, and any associated electronic transitions, are indicated by the lack of any large heat capacity anomalies accompanying the transitions.

This structural transition and related change in Coulomb landscape from 2D to 1D could explain some of the anomalies seen within the 270-290K temperature range: e.g. broad bump in susceptibility at 285K in $x=0.82$ [20], transition in optical ellipsometry at 280K in $x=0.82$ [21], phonon lifetime in infrared conductivity below 295K over a range of concentrations [22] and anomaly in resistivity [9, 23]. Further locking in of the dimensionality with electric field could lead to increased conductivity and improvement of the thermoelectric figure of merit. Of interest, in light of our results for $x = 0.78$, are the results of T.L. Schulze *et al.* in which a new magnetic transition is reported with slow cooling rate in $\text{Na}_{0.85}\text{CoO}_2$ indicating a coexistence of different sodium orderings, and therefore Coulomb landscapes, being frozen in with respect to fast cool [24].

In conclusion, striped phases have been observed in the sodium ordered temperature region. Below the transition temperature in our $\text{Na}_{0.78}\text{CoO}_2$ sample a phase coexistence is observed in a hexagon-of-hexagon superstructure pattern. This is explained by coexistence of a long range ordered trivacancy stripe along with a square trivacancy structure, as seen in $\text{Na}_{0.75}\text{CoO}_2$ and $\text{Na}_{0.92}\text{CoO}_2$. Above 285K these melt into a uncorrelated stripe structure for all three concentrations showing that this is a robust structure for this concentration range and temperature.

* Electronic address: jonathan.morris@hmi.de

- [1] I. Terasaki, Y. Sasago, and K. Uchinokura, Phys. Rev. B **56**, R12685 (1997).
- [2] Y. Wang et al., Nature **423**, 425 (2003).
- [3] K. Takada et al., Nature **422**, 53 (2003).
- [4] L. Helme et al., Phys. Rev. Lett. **94**, 157206 (2005).
- [5] S. Bayrakci et al., Phys. Rev. Lett. **94**, 157205 (2005).
- [6] J. Braconnier, C. Delmas, C. Fouassier, and P. Hagenmuller, Mat. Res. Bull. **15**, 1797 (1980).
- [7] H. Zandbergen et al., Phys. Rev. B **70**, 024101 (2004).
- [8] J. Geck et al., Phys. Rev. Lett. **97**, 106403 (2006).
- [9] M. Roger et al., Nature **445**, 631 (2007).
- [10] G. Shu et al., Phys. Rev. B **76**, 184115 (2007).
- [11] K. Takahata et al., Phys. Rev. B **61**, 12551 (2000).

- [12] Z. Ren et al., *J. Phys. Cond. Mat.* **18**, L379 (2006).
- [13] I. Mukhamedshin et al., *Phys. Rev. Lett.* **94**, 247602 (2005).
- [14] H. Alloul et al., *J. Phys. IV. France* **131**, 27 (2005).
- [15] D. Prabhakaran et al., *J. Crys. Growth* **271**, 74 (2004).
- [16] D. Prabhakaran and A. Boothroyd, *Frontiers in Superconducting Materials* (Springer-Verlag, Berlin, 2005), pp. 683–695.
- [17] D. Keen, M. Gutmann, and C. Wilson, *J. Appl. Cryst.* **39**, 714 (2006).
- [18] M. Gutmann, *SXD2001*, ISIS Facility, Rutherford Appleton Laboratory, Oxfordshire, UK. (2008).
- [19] C. Fouassier et al., *J. Solid State Chem.* **6**, 532 (1973).
- [20] S. Bayrakci et al., *Phys. Rev. B* **69**, 100410 (2005).
- [21] C. Bernhard et al., *Phys. Rev. Lett.* **93**, 167003 (2004).
- [22] S. Lupi et al., *Phys. Rev. B* **72**, 024550 (2005).
- [23] J. Wooldridge, D. Paul, G. Balakrishman, and M. Lees, *J. Phys.: Condens. Matter.* **17**, 707 (2005).
- [24] T. Schulze et al., *Phys. Rev. Lett.* **100**, 026407 (2008).

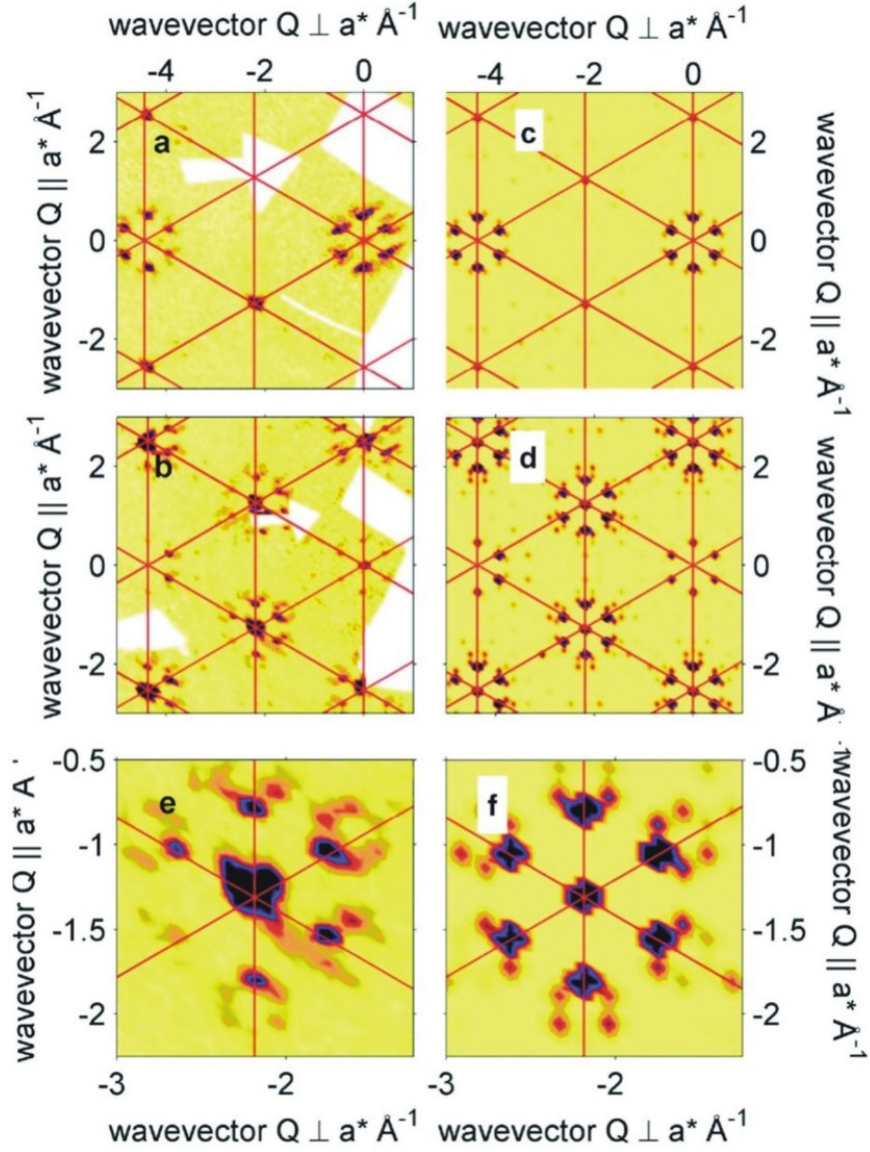


FIG. 1: (a-d) Top half of each panel shows neutron Laue diffraction data from SXD for $\text{Na}_{0.78}\text{CoO}_2$ for the $l=11$ and 7 planes respectively showing the hexagon-of-hexagons around the hexagonal structural Bragg peak positions along with the corresponding calculations mirrored in the bottom half of the panel. The calculation uses the phase coexistence of a square and stripe trivacancy phase showing good agreement with the data. (e, f) Detail of the $l=7$ plane showing good agreement between data and calculation.

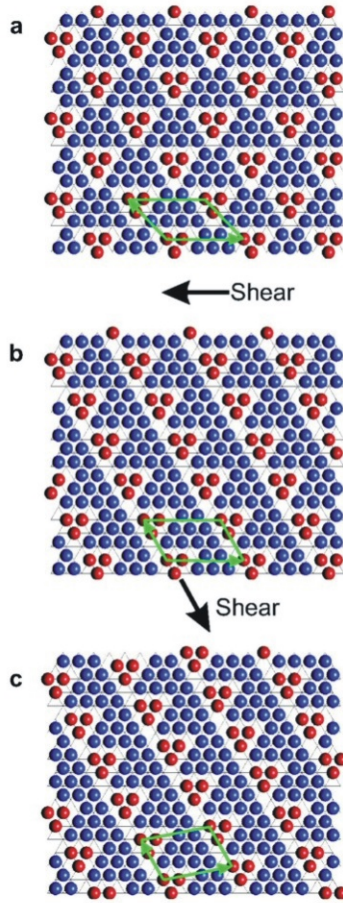


FIG. 2: a) The square trivacancy cluster structure seen in $\text{Na}_{0.75}\text{CoO}_2$ [9] requires a shear distortion parallel to the a -lattice direction to take it to (b) an unobserved stripe lattice and then a further shear along b to modify into (c) the stripe structure observed in $\text{Na}_{0.78}\text{CoO}_2$ data. (d) All three concentrations show the same phase above the melting transition at 285K, this is a disordered stripe structure.

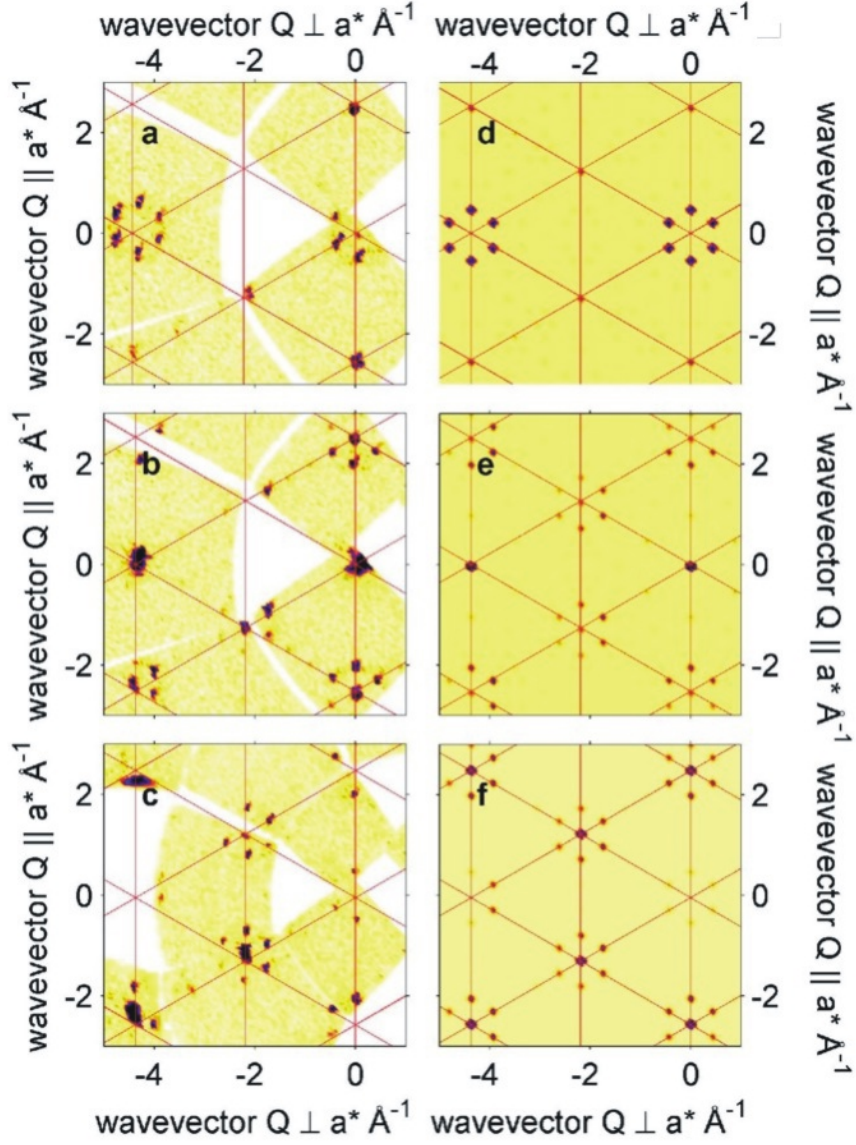


FIG. 3: Above 285K, in all three concentrations ($x=0.75, 0.78$ and 0.92), the long range ordered structure (figs. 2a, c) melt into one with disorder between stripes giving the same superstructure pattern (fig. 2d). a) $l=11$ for $\text{Na}_{0.92}\text{CoO}_2$ at 350K. (b) $l=10$ and (c) $l=7$ showing the l dependence. d-f) Calculation using the disordered stripe structure. Note the in plane intensity modulation is captured in the simulation.

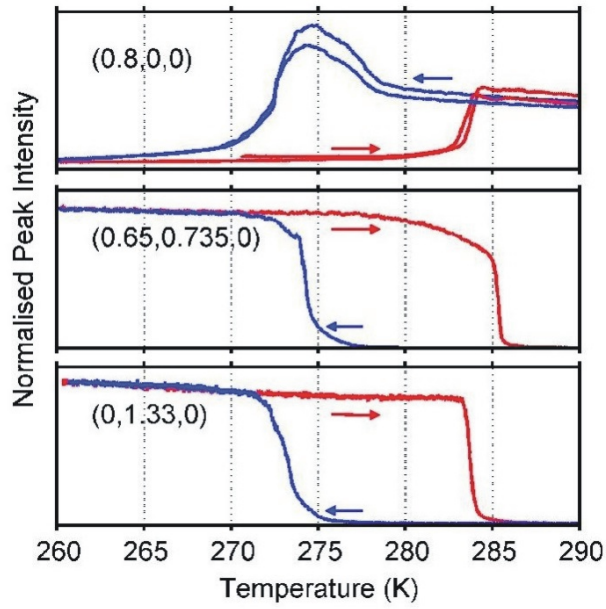


FIG. 4: Hysteresis behaviour of the order to disordered stripe transition in the intensities of superstructure peaks measured using hard x-ray diffraction on $x=0.75$.